Mem. S.A.It. Suppl. Vol. 22, 152

Memorie della
Supplementi

^{6}Li detection in metal-poor stars: can 3D model atmospheres solve the second lithium problem?

M. Steffen[1,2], R. Cayrel[2], E. Caffau[3,2], P. Bonifacio[2], H.-G. Ludwig[3,2], and M. Spite[2]

[1] Leibniz-Institut für Astrophysik Potsdam (AIP), An der Sternwarte 16, 14482 Potsdam, Germany, e-mail: msteffen@aip.de
[2] GEPI Observatoire de Paris, CNRS, Universite Paris Diderot, F-92195 Meudon Cedex, France
[3] Zentrum für Astronomie der Universität Heidelberg, Landessternwarte, Königstuhl 12, 69117 Heidelberg, Germany

Abstract. The presence of ^{6}Li in the atmospheres of metal-poor halo stars is usually inferred from the detection of a subtle extra depression in the red wing of the ^{7}Li doublet line at 670.8 nm. However, as pointed out recently by Cayrel et al. (2007), the intrinsic line asymmetry caused by convective flows in the photospheres of cool stars is almost indistinguishable from the asymmetry produced by a weak ^{6}Li blend on a (presumed) symmetric ^{7}Li profile. Previous determinations of the ^{6}Li/ ^{7}Li isotopic ratio based on 1D model atmospheres, ignoring the convection-induced line asymmetry, must therefore be considered as upper limits. By comparing synthetic 1D LTE and 3D non-LTE line profiles of the Li I 670.8 nm feature, we quantify the differential effect of the convective line asymmetry on the derived ^{6}Li abundance as a function of effective temperature, gravity, and metallicity. As expected, we find that the asymmetry effect systematically reduces the resulting ^{6}Li/^{7}Li ratios. Depending on the stellar parameters, the 3D-1D offset in ^{6}Li/^{7}Li ranges between -0.005 and -0.020. When this purely theoretical correction is taken into account for the Asplund et al. (2006) sample of stars, the number of significant ^{6}Li detections decreases from 9 to 5 (2σ criterion), or from 5 to 2 (3σ criterion).
We also present preliminary results of a re-analysis of high-resolution, high S/N spectra of individual metal-poor turn-off stars, to see whether the *second Lithium problem* actually disappears when accounting properly for convection and non-LTE line formation in 3D stellar atmospheres. Out of 8 stars, HD 84937 seems to be the only significant (2σ) detection of ^{6}Li. In view of our results, the existence of a ^{6}Li plateau appears questionable.

Key words. stars: abundances - stars: atmospheres – convection – line: profiles – stars: population II - stars: individual: (HD 74000, HD 84937, HD 140283, HD 160617, G271-162, G020-024, G64-12, G275-4)

1. Introduction

A systematic analysis of high-dispersion, high signal-to-noise (S/N) UVES and Keck spectra of about 30 bright metal-poor stars by Asplund et al. (2006) and Asplund & Melendez (2008) (henceforth A06 and A08, respectively) resulted in the detection of ^{6}Li (at the $2\,\sigma$ level) in about one third of these objects. The average ^{6}Li/^{7}Li isotopic ratio in the stars in which ^{6}Li

has been detected is about 4% and is very similar in each of these stars, defining a ^{6}Li plateau at approximately $\log n(^6\mathrm{Li})/n(\mathrm{H}) + 12 = 0.85$. A convincing theoretical explanation of this new ^{6}Li plateau turned out to be problematic: the high abundance of ^{6}Li at the lowest metallicities cannot be explained by current models of galactic cosmic-ray production, even if the depletion of ^{6}Li during the pre-main-sequence phase is ignored (see reviews by e.g. Cayrel et al. 2008; Christlieb 2008; Prantzos 2010, 2012, and references therein).

A possible solution of this so-called *second Lithium problem* was proposed by Cayrel et al. (2007): noting that the spectroscopic signature of the presence of ^{6}Li in the atmospheres of metal-poor halo stars is just a subtle extra depression in the red wing of the ^{7}Li doublet, which is difficult to measure even in spectra of the highest quality, they point out that the intrinsic line asymmetry caused by convection in the photospheres of cool stars closely mimics the presence of ^{6}Li at the level of a few percent if interpreted in terms of 1D, intrinsically symmetric blend components. As a consequence, the ^{6}Li abundance derived so far by using 1D model atmospheres, ignoring the convective line asymmetry, are expected to be systematically too high.

We quantify the theoretical effect of the convection-induced line asymmetry on the resulting ^{6}Li abundance by fitting a given synthetic profile both with a grid of 1D LTE and a grid of 3D non-LTE line profiles. The 1D-3D difference of the required ^{6}Li/^{7}Li isotopic ratio measures the expected systematic error in ^{6}Li/^{7}Li inherent to the standard 1D analysis. The synthetic spectra used for this differential comparison are based on a set of 3D hydrodynamical model atmospheres computed with the CO^{5}BOLD code (Freytag et al. 2002, 2012) and a corresponding set of fully compatible 1D mixing-length models, respectively, as outlined in Sect. 2. The results of this investigation may be represented by an analytical approximation, giving the 3D correction of ^{6}Li/^{7}Li as a function of effective temperature, gravity, and metallicity, for a parameter range that covers the stars of the A06 sample (Sect. 3). We also discuss the potential advantages and disadvantages of using so called 'calibration lines' for fixing the residual line broadening, and show that the usage of such 'calibration lines' is potentially dangerous, because the inferred broadening parameter shows considerable line-to-line variations. Depending on the choice of these lines, the resulting ^{6}Li abundance may be systematically biased (Sect. 4).

A careful reanalysis of individual objects is under way to see whether the *second Lithium problem* can be resolved when accounting properly for convection and non-LTE line formation in 3D stellar atmospheres. In Sect. 5 we present a preliminary analysis of eight individual metal-poor turn-off stars for which sufficiently high-resolution, high S/N spectra are at our disposal, fitting the observed Li I 670.8 nm feature with both 1D LTE and 3D non-LTE synthetic line profiles. As expected, the 3D analysis gives a systematically lower ^{6}Li/^{7}Li ratio by roughly 0.01 with respect to the 1D result. In most cases, we find that the detection of ^{6}Li is not significant at the 2σ level.

2. 3D model atmospheres and spectrum synthesis

The hydrodynamical atmospheres used in the present study are part of the CIFIST 3D model atmosphere grid (Ludwig et al. 2009). They have been obtained from realistic numerical simulations with the CO^{5}BOLD code[1] (Freytag et al. 2002, 2012) which solves the time-dependent equations of compressible hydrodynamics in a constant gravity field together with the equations of non-local, frequency-dependent radiative transfer in a Cartesian box representative of a volume located at the stellar surface. The computational domain is periodic in x and y direction, has open top and bottom boundaries, and is resolved by typically 140×140×150 grid cells. The vertical optical depth of the box varies typically from $\log \tau_{\mathrm{Ross}} \approx -7.0$ (top) to $\log \tau_{\mathrm{Ross}} \approx +7.5$ (bottom). Further information about the grid of models used in the present study is compiled in Table 1. As indicated in

[1] http://www.astro.uu.se/~bf/co5bold_main.html

columns (2) – (4), the grid covers the range 5900 K $\leq T_{\rm eff} \leq$ 6500 K, 3.5 $\leq \log g \leq$ 4.5, $-3.0 \leq$ [Fe/H] $\leq$ 0.0. Radiative transfer is solved in 5 or 6 opacity bins (col. 5). Each of the models is represented by typically 20 snapshots chosen from the full time sequence of the corresponding simulation (col. 6).

These representative snapshots are processed by the non-LTE code NLTE3D that solves the statistical equilibrium equations for a 17 level lithium atom with 34 line transitions, fully taking into account the 3D thermal structure of the respective model atmosphere (but neglecting the differential Doppler shifts implied by the hydrodynamical velocity field). The photo-ionizing radiation field is computed at 704 frequency points between λ 925 and 32 407 Å, using the opacity distribution functions of Castelli & Kurucz (2003) to allow for metallicity-dependent line-blanketing, including the H I–H$^+$ and H I–H I quasi-molecular absorption near λ 1400 and 1600 Å, respectively. Collisional ionization by neutral hydrogen via the charge transfer reaction H($1s$) + Li($n\ell$) $\leftrightarrow$ Li$^+$($1s^2$) + H$^-$ is treated according to Barklem, et al. (2003). More details are given in Sbordone et al. (2010). Finally, 3D non-LTE synthetic line profiles of the Li I λ 670.8 nm doublet are computed with the line formation code Linfor3D[2], using the departure coefficients $b_i = n_i$(NLTE)$/n_i$(LTE) provided by NLTE3D for each level i of the lithium model atom as a function of geometrical position within the 3D model atmospheres. At this stage, the 3D hydrodynamical velocity field provides the differential line shifts along each line of sight. As demonstrated in Steffen et al. (2010b), non-LTE effects are very important for the 3D models of the metal-poor dwarfs considered here: they strongly reduce the height range of line formation such that the 3D non-LTE equivalent width is smaller by roughly a factor 2 compared to 3D LTE. Ironically, the line strength predicted by standard 1D mixing-length models in LTE are close to the results obtained from elaborate 3D non-LTE calculations. Nevertheless, when it comes to the determination of the ^{6}Li/^{7}Li isotopic ratio, it is important to account for the convective line asymmetry, which requires the full 3D non-LTE line formation calculations.

[2] http://www.aip.de/~mst/linfor3D_main.html

3. Theoretical 3D non-LTE correction of 1D LTE ^{6}Li/^{7}Li determinations

As outlined above, the ^{6}Li abundance is systematically overestimated if the intrinsic asymmetry of the ^{7}Li line components is ignored. To quantify this bias theoretically, we rely on synthetic spectra. The idea is as follows: we represent the observation by the synthetic 3D non-LTE line profile of the ^{7}Li line blend, computed with zero ^{6}Li content. The non-thermal line broadening is naturally provided by the 3D hydrodynamical velocity field, which replaces the classical concept of micro- and macroturbulence, and also gives rise to a convective blue-shift and an intrinsic line asymmetry. Optionally, the line blend is subsequently broadened by rotation ($v \sin i$) and a Gaussian instrumental profile ($FWHM$ denoting its full width at half maximum). Now this realistic proxy of the ^{7}Li line blend is fitted by a grid of 'classical' 1D LTE synthetic line profiles. The 1D LTE line profiles are computed from so-called LHD models, 1D mixing-length model atmospheres that have the same stellar parameters and employ the same microphysics and radiative transfer scheme as the corresponding 3D model, assuming a mixing-length parameter of $\alpha_{\rm MLT} = 0.5$, and a depth-independent microturbulence of $\xi_{\rm mic} = 1.5$ km/s.

Five parameters are varied independently until the best fit is found (χ^2 minimization): in addition to the total ^{6}Li+^{7}Li abundance, A(Li), and the isotopic ratio, q(Li)=^{6}Li/^{7}Li, which control line strength and line asymmetry, respectively, we also allow for a residual line broadening described by a Gaussian kernel with half-width $V_{\rm BR}$, a global line shift, Δv, and a global scaling of the continuum level, $S_{\rm c}$. For technical reasons, the rotational line broadening is not treated as a fitting parameter; it is fixed to the value used in the 3D spectrum synthesis.

Note that, although the five fitting parameters are correlated, each one has a distinctly

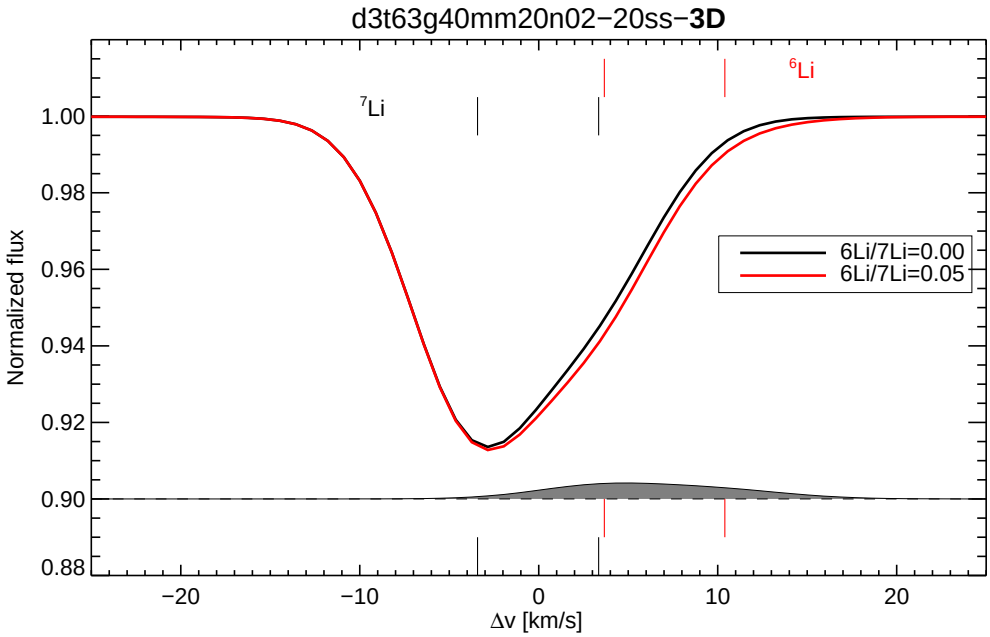

Fig. 1. Example of a 3D non-LTE synthetic profile of the Li I 670.8 nm feature, for stellar parameters $T_{\rm eff}$ = 6300 K, $\log g$ = 4.0, [Fe/H]=-2. Increasing the ^{6}Li content from 0 to 5% leads to an extra depression of the red wing by about 0.5% (indicated by the gray area), leaving the blue wing unaffected. In order to detect such a small effect, observed spectra are required to have an S/N in excess of ≈ 400.

different effect on the line profile. The broadening $V_{\rm BR}$ is fixed by the slope of the blue wing, which is not affected by the ^{6}Li content, (see Fig. 1), while q(Li) is fixed by the shape of the red wing. This allows to obtain unambiguously a unique solution although a given half width of the line blend can be obtained by different combinations of q(Li) and $V_{\rm BR}$, but with higher χ^2 values than the best solution.

Finally, the 3D non-LTE correction of the ^{6}Li/^{7}Li isotopic ratio is defined as the difference between the values of q(Li) that provide the best fit (*) to the given profile using 1D LTE and 3D non-LTE profiles, respectively: Δq(Li) = $q^*_{\rm (1D\,LTE)}$(Li) - $q^*_{\rm (3D\,NLTE)}$(Li)[3]. This differential correction is meant to be *subtracted* from the ^{6}Li/^{7}Li isotopic ratio derived from the 1D LTE analysis to correct for the bias introduced by neglecting the intrinsic line asymmetry: $q_{\rm (3D\,NLTE)}$(Li) = $q_{\rm (1D\,LTE)}$(Li) - Δq(Li). Note that this correction procedure properly accounts for radiative transfer in the lines, including saturation effects.

We have determined Δq(Li) according to the method outlined above for each of the 3D model atmospheres in our grid, considering two cases: $\Delta q_{\rm (A)}$(Li) and $\Delta q_{\rm (B)}$(Li) are the result of fitting the unprocessed ($v \sin i$ = 0.0 km/s, $FWHM$ = 0.0 km/s) and the broadened ($v \sin i$ = 1.5 km/s, $FWHM$ = 2.5 km/s) synthetic line profile, respectively. Case (B) is the more realistic one, while case (A) has been included only to show how the amount of instrumental broadening is affecting the amplitude of Δq(Li). Note also that the 3D corrections given in previous studies by (Steffen et al. 2010a,b) correspond to case (A).

The results of this computationally very expensive procedure are given in cols. (8) and (9) of Table 1. They may be aproximated fairly

[3] $q^*_{\rm (3D\,NLTE)}$(Li) is zero by construction here

Table 1. List of 3D models used in the present study. Columns (2)-(6) give effective temperature, surface gravity, metallicity, number of opacity bins used in the radiation hydrodynamics simulation, and number of snapshots selected for spectrum synthesis. The equivalent width of the synthetic 3D non-LTE ^{7}Li doublet at λ 670.8 nm, assuming A(Li)=2.2 and no ^{6}Li, is given in col. (7). Columns (8) and (9) show $\Delta q_{(\mathrm{A})}$(Li) and $\Delta q_{(\mathrm{B})}$(Li), the 3D non-LTE correction of the ^{6}Li/^{7}Li isotopic ratio inferred from fitting the unprocessed (no rotational and instrumental broadening) and the broadened ($v \sin i$ = 1.5 km/s, $FWHM$ = 2.5 km/s) 3D non-LTE line profile, respectively, with a grid of 1D LTE profiles.

Model	$T_{\rm eff}$ [1)] [K]	log g	[Fe/H]	Nbin	Nsnap	W [2)] [mÅ]	Δq(Li)=$q^*_{(\mathrm{1D\,LTE})}$(Li) [×100] (A)	(B)
d3t59g35mm30n01	5873	3.5	-3.0	6	20	41.7	2.13	1.99
d3t59g40mm30n02	5846	4.0	-3.0	6	20	44.9	0.88	0.86
d3t59g45mm30n01	5924	4.5	-3.0	6	19	39.9	0.63	0.61
d3t63g35mm30n01	6306	3.5	-3.0	6	20	21.7	3.44	3.12
d3t63g40mm30n01	6269	4.0	-3.0	6	20	23.9	1.51	1.38
d3t63g45mm30n01	6272	4.5	-3.0	6	18	24.3	0.85	0.80
d3t65g40mm30n01	6408	4.0	-3.0	6	20	20.0	1.70	1.56
d3t65g45mm30n01	6556	4.5	-3.0	6	12	16.4	1.25	1.16
d3t59g35mm20n01	5861	3.5	-2.0	6	20	42.8	1.88	1.76
d3t59g40mm20n02	5856	4.0	-2.0	6	20	45.2	0.73	0.69
d3t59g45mm20n01	5923	4.5	-2.0	6	18	42.3	0.45	0.41
d3t63g35mm20n01	6287	3.5	-2.0	6	20	22.1	4.04	3.75
d3t63g40mm20n01	6278	4.0	-2.0	6	16	23.7	1.48	1.35
d3t63g45mm20n01	6323	4.5	-2.0	6	19	23.0	0.94	0.88
d3t65g40mm20n01	6534	4.0	-2.0	6	19	16.2	2.22	2.01
d3t65g45mm20n01	6533	4.5	-2.0	6	19	17.0	1.21	1.12
d3t59g35mm10n02	5890	3.5	-1.0	6	20	38.0	2.91	2.71
d3t59g40mm10n02	5850	4.0	-1.0	6	20	41.5	1.45	1.36
d3t59g45mm10n01	5923	4.5	-1.0	6	08	38.2	0.83	0.76
d3t63g35mm10n01	6210	3.5	-1.0	6	20	23.0	4.57	4.18
d3t63g40mm10n01	6261	4.0	-1.0	6	20	22.0	2.33	2.15
d3t63g45mm10n01	6238	4.5	-1.0	6	20	23.4	1.23	1.14
d3t65g40mm10n01	6503	4.0	-1.0	6	20	15.5	3.14	2.82
d3t65g45mm10n01	6456	4.5	-1.0	6	19	17.1	1.44	1.33
d3t59g35mm00n01	5884	3.5	0.0	5	20	33.0	3.37	3.06
d3t59g40mm00n01	5928	4.0	0.0	5	18	31.1	1.83	1.70
d3t59g45mm00n01	5865	4.5	0.0	5	19	34.7	1.15	1.06
d3t63g40mm00n01	6229	4.0	0.0	5	20	19.1	2.66	2.43
d3t63g45mm00n01	6233	4.5	0.0	5	20	19.3	1.49	1.47
d3t65g40mm00n01	6484	4.0	0.0	5	20	12.8	3.88	3.55
d3t65g45mm00n01	6456	4.5	0.0	5	20	13.8	1.75	1.61

Notes: [1)] averaged over selected snapshots; [2)] averaged over selected 3D non-LTE spectra

well by the following polyonmial expression:

$$\Delta q_{(\mathrm{B})}(\mathrm{Li})\{T_{\rm eff}, \log g, [\mathrm{Fe/H}]\} = a_{00} + a_{01}\,Z + (a_{10} + a_{11}\,Z)\;Y + (a_{20} + a_{21}\,Z)\;Y^2 + (a_{30} + a_{31}\,Z)\;X + (a_{40} + a_{41}\,Z)\;X\,Y + \left(a_{50} + a_{51}\,Z + a_{52}\,Z^2\right)\;X^2 \quad (1)$$

where $X \equiv (T_{\rm eff} - 6300)/1000$, $Y \equiv \log g - 4.0$, and $Z \equiv$[Fe/H]+2. The coefficients a_{ij} are listed in Table 2. Contour plots of this polynomial approximation are shown in Fig. 2.

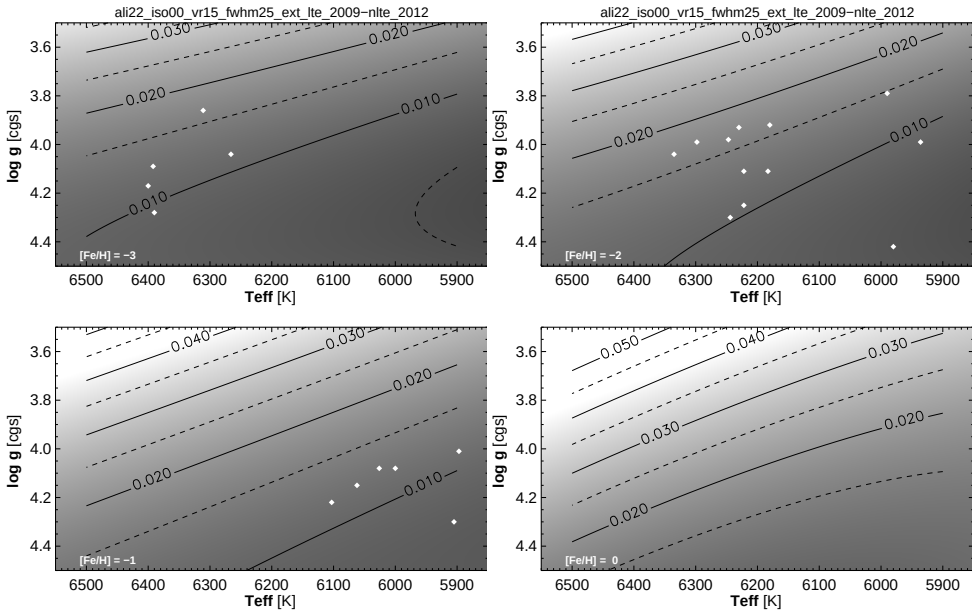

Fig. 2. Contours of $\Delta q_{(\mathrm{B})}$(Li) in the $T_{\mathrm{eff}} - \log g$ plane at constant metallicity [Fe/H] = −3, −2, −1, and 0, respectively (from top left to bottom right) according to the approximation given by Eq. (1) and Table 2. White symbols mark the positions of the stars from the A06 sample with Fe/H] < −2.5 (top left), −2.5 < [Fe/H] < −1.5 (top right), and −1.5 < [Fe/H] < −0.5 (bottom left).

Table 2. Coefficients a_{ij} representing $\Delta q_{(\mathrm{B})}$(Li) as a function of T_{eff}, $\log g$, and [Fe/H] according to Eq. (1).

j	$a_{0\mathrm{j}} \times 100$	$a_{1\mathrm{j}} \times 100$	$a_{2\mathrm{j}} \times 100$
0	1.6984	0.4311	0.0000
1	-2.6658	-0.4547	0.0000
2	2.3370	-0.3211	0.0000
3	2.3490	0.6300	0.0000
4	-2.7366	-0.6089	0.0000
5	0.1786	0.5657	0.5385

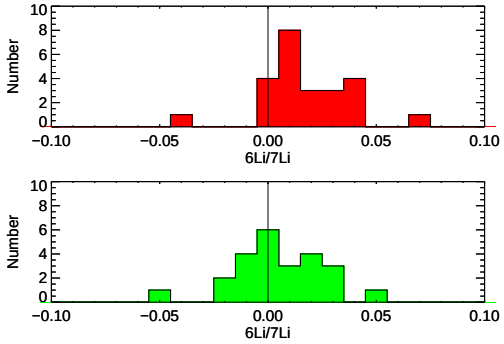

Fig. 3. Histogram of the ^{6}Li/^{7}Li determinations by A06 before (top) and after (bottom) application of the 3D correction $\Delta q_{(\mathrm{B})}$(Li).

At given metallicity, the corrections are largest for low gravity and high effective temperature. They increase towards higher metallicity. Note that the corrections are strictly valid only for a Li abundance of A(Li)=2.2. The results for [Fe/H]=0.0 are most uncertain, since they are based on fewer data points.

The analysis of A06 utilizes 1D LTE profiles computed from MARCS model atmospheres. Hence, the correction $\Delta q_{(B)}$(Li) should be applied to their ^{6}Li/^{7}Li isotopic ratios. The resulting downward corrections are typically in the range 1% < $\Delta q_{(B)}$(Li) < 2% for the stars of their sample (cf. Fig. 2). After subtracting

the individual $\Delta q_{(B)}$(Li) for each of these stars, interpolated via Eq. (1) to their $T_{\rm eff}$, $\log g$, and [Fe/H], the mean ^{6}Li/^{7}Li isotopic ratio of the sample is reduced from 0.0212 to 0.0088. The center of the distribution of ^{6}Li/^{7}Li is shifted essentially to zero (see Fig. 3).

Based on the original ^{6}Li/^{7}Li isotopic ratios and their 1σ error bars as determined by A06, the number of stars with a ^{6}Li detection above the 2σ and 3σ level is 9 and 5, respectively, out of 24. After correction, the number of 2σ and 3σ detections is reduced to 5 and 2, respectively. The 3σ detections after correction are HD 106038 and G020−024, the remaining 2σ detections are HD 102200, HD 160617, and CD−30 18140.

We note that HD 106038 survives as a 3σ detection only because of its amazingly small error bar of ±0.006. Assuming a more typical error of ±0.013, this object would not even qualify as a 2σ detection. HD 102200 seems to be a clear 2σ detection (q(Li) = 0.036 ± 0.013), while CD−30 18140 is a marginal case (q(Li) = 0.029 ± 0.013). The remaining objects, G020-024 and HD 160617, are discussed in more detail in Sect. 5, where their spectra are reanalyzed with 3D non-LTE line profiles; none of them provides convincing evidence for the presence of ^{6}Li.

4. Fixing the residual line broadening by 'calibration lines'

So far we have derived all information from fitting the Li 670.8 nm feature, for which we have a 3D non-LTE line formation model. In principle, the accuracy of the fitting procedure can be improved by fixing the value of the residual line broadening, $V_{\rm BR}$, from additional unblended 'calibration lines'. This approach has been adopted by A06 (see also Lind et al. 2012, henceforth L12). This fact complicates the comparison with our results, and the correction procedure described in Sect. 3 explains only part of the differences. We show in the following that 'calibration lines' may introduce additional uncertainties, unless their 3D non-LTE line formation is fully understood.

In the framework of 1D models, $V_{\rm BR}$, represents the combined effect of macroturbulence and instrumental broadening (for given microturbulence and rotational velocity) and is expected to be independent of the spectral line. In general, an average value of $V_{\rm BR}$ from several calibration lines is then used for the analysis of the Li line, thus reducing the number of free fitting parameters, and hence the formal errors of the fitting results.

We have simulated this procedure using synthetic lines only. Our selection of 10 calibration lines is compiled in Tab. 3. The lines have been selected to have similar wavelength, equivalent width, and excitation energy (relative to the ionization continuum) as Li I 670.8 nm. Synthetic line profiles generated from 3D model d3t63g40mm20n01 (assuming LTE) represent the observed line profiles and are fitted with 1D LTE profiles from the corresponding LHD model to derive $V_{\rm BR}$. The results are given in col. (5) of Tab. 3. These numbers have to be compared with the value of $V_{\rm BR}$ obtained by fitting the 3D non-LTE Li profile of the same 3D model with 1D LTE pro-

Table 3. List of calibration lines. Columns (2) to (4) show their wavelength, excitation potential, and equivalent width. The residual line broadening derived from 1D LTE fitting and the resulting error of ^{6}Li/^{7}Li is given in cols. (5) and (6). The last row refers to the Li line; cols. (5) and (6) show the results of 3D non-LTE fitting without calibration lines.

Ion	λ [nm]	$E_{\rm i}$ [eV]	W_λ [pm]	$V_{\rm BR}$ [kms]	$\delta q^{(1D)}$ [×100]
Fe I	538.337	4.312	2.74	4.88	0.35
Fe I	606.548	2.608	1.38	4.63	1.25
Fe I	613.662	2.453	2.47	4.52	1.64
Fe I	613.769	2.588	1.87	4.59	1.39
Fe I	623.072	2.559	2.51	4.54	1.57
Fe I	625.256	2.404	1.64	4.56	1.50
Fe I	639.360	2.433	2.53	4.51	1.67
Fe I	649.498	2.404	3.54	4.39	2.08
Fe I	667.799	2.692	1.58	4.62	1.29
Ca I	671.768	2.709	0.78	4.83	0.53
Li I	670.784	0.000	2.37	4.97	0.00

Table 4. List of observed Li I λ 670.8 nm spectra of eight metal-poor turn-off stars, analyzed in this work for the presence of ^{6}Li.

Star	$T_{\rm eff}$ [K]	log g	[Fe/H]	R=$\lambda/\Delta\lambda$	S/N *)	Instrument	Reference
HD 74000	6203	4.03	-2.05	120 000	600	ESO3.6 / HARPS	C07 1)
G271−162	6330	4.00	-2.25	110 000	600	VLT / UVES	N00 2)
HD 84937	6310	4.10	-2.40	100 000	650	CFHT / GECKO	C99 3)
G020−024	6247	3.98	-1.89	120 000	420	VLT / UVES	A06 4)
HD 140283	5753	3.70	-2.40	95 000	1000	SUBARU / HDS	A04 5)
HD 160617	5990	3.79	-1.76	100 000	400	ESO3.6 / HARPS	M12 6)
G64−12	6371	4.26	-3.24	95 000	620	Keck / HIRES	A08 7)
G275−4	6338	4.32	-3.21	93 000	700	VLT / UVES	N09 8)

Notes: 1) Cayrel et al. (2007), 2) Nissen et al. (2000), 3) Cayrel et al. (1999), 4) Asplund et al. (2006), 5) Aoki et al. (2004), 6) L. Monaco and G. Lo Curto (2012, priv. comm.), 7) Asplund & Melendez (2008), 8) P.E. Nissen (2009, priv. comm.),
*) S/N estimated from the (re-reduced) spectra actually used in this work, may differ from literature values.

files from LHD models, $V_{\rm BR}$ = 4.97 km/s (last row of Tab. 3). When fixing $V_{\rm BR}$ to the values implied by the individual calibration lines, the resulting ^{6}Li/^{7}Li isotopic ratio changes by $\delta q^{(1D)}$(Li) with respect to the value obtained when treating $V_{\rm BR}$ as a free fitting parameter.

We find that, even under these idealized conditions, $\delta q^{(1D)}$(Li) is not constant but varies from line to line (see col. (6) of Tab. 3). This is an indication that 1D micro / macro model is not perfectly adequate to describe the 3D hydrodynamical velocity field. Moreover, since $\delta q^{(1D)}$(Li) is positive for all of our calibration lines, the use of calibration lines leads to an additional overestimation of the Li isotopic ratio by up to 2%. The total error of the 1D analysis is obtained by adding the corrections from Tables 1 and 3, Δq(Li) = $\Delta q_{(B)}$(Li) + $\delta q^{(1D)}$(Li).

In a further experiment, we have fitted both the calibration lines and the Li feature with 3D LTE line profiles. By construction, the derived $V_{\rm BR}$ is then equal to $FWHM$ of the assumed instrumental profile, and is identical for all calibration lines. The Li isotopic ratio obtained from fitting the 3D non-LTE Li feature with 3D LTE profiles and fixed $V_{\rm BR}$ = $FWHM$ is $\delta q^{(3D)}$(Li)=0.054, compared to 0.003 if $V_{\rm BR}$ is a free fitting parameter. The basic reason for this alarming result is that the half width of the Li line is significantly smaller in LTE than in non-LTE, which must be compensated by a higher ^{6}Li content. This effect may explain why A06 find higher ^{6}Li/^{7}Li isotopic ratios in their 3D LTE analysis (with respect to 1D LTE, their Table 5).

We note that the above results are consistent with previous findings by Steffen et al. (2010b), who analyzed the spectrum of HD 74000 with a subset of 6 clean Fe I calibration lines, and obtained significantly higher ^{6}Li/^{7}Li isotopic ratios compared to the analysis without calibration lines. The same behavior is seen by L12, if they fit both the calibration lines and Li with 3D LTE profiles. Using instead non-LTE profiles for fitting both Ca I and Li I lines leads to consistent ^{6}Li/^{7}Li isotopic ratios for HD 84937.

5. Analysis of observed spectra: 3D non-LTE versus 1D LTE line fitting

With the results given in Sect. 3, the recommended method of analysis of the Li I 670.8 nm doublet in an observed spectrum is as follows. The first step is to produce a grid of 1D LTE synthetic line profiles as a function of A(Li), q(Li), using any standard 1D mixing-length model with the correct stellar parameters ($T_{\rm eff}$, log g, [Fe/H]). This grid is then used to find the best fit to the observed line profile, as described above (no calibration lines). Finally, the resulting q(Li) is corrected for 3D effects by subtracting the differential correction $\Delta q_{(B)}$(Li) defined in Sect. 3, interpolated to the actual stellar parameters according to Eq. (1) and Table 2.

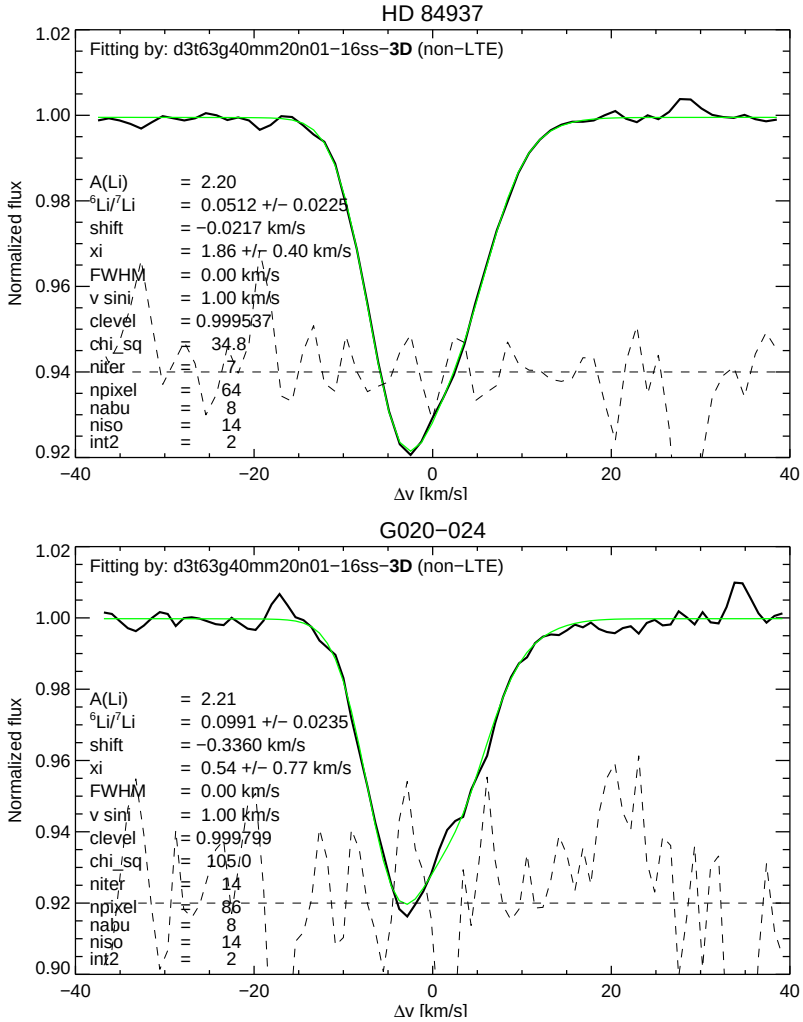

Fig. 4. The best fitting 3D non-LTE Li 670.8 nm line profile (green) superimposed on the observed spectrum (solid black) of HD 84937 (top) and G020–024 (bottom). The difference between computed and observed spectrum (×10; dashed line) indicates the quality of the fit, which is much better for HD 84937 than for G020–024, the latter suffering from a 'perturbation' in its lower red wing.

In the following, however, we disregard this differential approach, and present instead preliminary results of fitting the observed Li I λ 670.8 nm spectra of eight halo turn-off stars (see Table 4) directly with our grids of 3D non-LTE and 1D LTE synthetic line profiles, computed from 3D CO^{5}BOLD models and 1D LHD models, respectively. As described above, five free fitting parameters (A(Li), q(Li), $V_{\rm BR}$, Δv, $S_{\rm c}$) are varied independently to find the best fit. Formally, we fix the rotational velocity to $v \sin i$=1.0 km/s, noting that the derived ^{6}Li/^{7}Li isotopic ratio is insensitive to this assumption (see Steffen et al. 2010b).

The results are presented in Table 5. The errors quoted for $V_{\rm BR}$ and q(Li) are the formal 1 σ confidence intervals due to the finite S/N of the fitted spectra. They are computed in the usual way (see e.g. Nissen et al. 2000; Asplund et al. 2006) by finding the distance Δp of the

Table 5. Fitting the observed spectra of Table 4 with 3D non-LTE and 1D LTE line profiles.

Star	Model name	synthetic spectrum	A(Li) [1]	$V_{\rm BR}$ [2] [km/s]	q(Li) this work	[×100] A06,A08,L12
HD 74000	d3t63g40mm20n01	3D NLTE	2.25	2.9 ± 0.4	−0.8 ± 1.2	—
	t6280g40mm20a05ob6	1D LTE	2.23	5.7 ± 0.2	0.6 ± 1.1	—
G271−162	d3t63g40mm20n01	3D NLTE	2.29	3.5 ± 0.3	0.6 ± 1.1	—
	t6280g40mm20a05ob6	1D LTE	2.27	6.1 ± 0.2	2.1 ± 1.2	1.9 ± 1.2 [3]
HD 84937	d3t63g40mm20n01	3D NLTE	2.20	3.1 ± 0.7	5.1 ± 2.3	0.7 ± 0.5 [5]
	t6280g40mm20a05ob6	1D LTE	2.18	5.8 ± 0.4	6.6 ± 2.4	—
G020−024	d3t63g40mm20n01	3D NLTE	2.21	0.9 ± 1.3	9.9 ± 2.4	—
	t6280g40mm20a05ob6	1D LTE	2.19	5.0 ± 0.4	11.7 ± 2.5	7.0 ± 1.7 [3]
HD 140283	d3t57g37mm20n01	3D NLTE	2.20	3.7 ± 0.1	−0.6 ± 0.4	−0.4 ± 0.2 [5]
	d3t57g37mm30n01	3D NLTE	2.22	3.3 ± 0.1	−1.0 ± 0.4	—
	t5775g37mm20ml3a05ob6	1D LTE	2.18	5.5 ± 0.1	0.5 ± 0.4	0.8 ± 0.6 [3]
	t5789g37mm30ml3a05ob6	1D LTE	2.19	5.5 ± 0.1	0.4 ± 0.4	—
HD 160617	d3t59g40mm20n02	3D NLTE	2.14	4.5 ± 0.2	−0.5 ± 1.2	—
	d3t59g35mm20n01	3D NLTE	2.17	3.3 ± 0.3	−1.3 ± 1.2	—
	t5860g40mm20ml3a05	1D LTE	2.11	5.8 ± 0.2	0.1 ± 1.2	3.6 ± 1.0 [3]
	t5860g35mm20a05	1D LTE	2.13	5.8 ± 0.2	0.3 ± 1.2	—
G64−12	d3t63g40mm30n01	3D NLTE	2.19	5.0 ± 0.5	0.8 ± 2.7	2.1 ± 1.2 [5]
	d3t63g45mm30n01	3D NLTE	2.19	5.5 ± 0.5	1.2 ± 2.8	—
	t6270g40mm30ml3a05	1D LTE	2.16	7.1 ± 0.4	2.3 ± 2.9	5.9 ± 2.1 [4]
	t6270g45mm30ml3a05ob6	1D LTE	2.14	7.0 ± 0.4	2.0 ± 2.9	—
G275−4	d3t63g40mm30n01	3D NLTE	2.11	3.6 ± 0.6	3.5 ± 2.4	—
	d3t63g45mm30n01	3D NLTE	2.11	4.3 ± 0.5	3.8 ± 2.4	—
	t6270g40mm30ml3a05	1D LTE	2.08	6.3 ± 0.4	4.7 ± 2.5	—
	t6270g45mm30ml3a05ob6	1D LTE	2.06	6.2 ± 0.4	4.4 ± 2.4	—

Notes: [1] $\log\left[n(^6\mathrm{Li}) + n(^7\mathrm{Li})\right] - \log n(\mathrm{H}) + 12$; [2] Gaussian kernel, [3] Asplund et al. (2006), [4] Asplund & Melendez (2008), [5] Lind et al. (2012)

parameter of interest p from is optimum value p_0 such that $\chi^2(p + \Delta p) - \chi^2(p_0) \equiv \Delta\chi^2 = 1$, fixing p and minimizing $\Delta\chi^2$ over the remaining free fittting parameters. Here χ^2 is defined as

$$\chi^2 = \sum_i \frac{(O_i - S_i)^2}{\sigma^2}\,, \qquad (2)$$

where O_i and S_i are the observed and synthetic flux at wavelength point i, and σ=(S/N)$^{-1}$, with S/N taken from Tab. 4. Note that this is a lower limit to the real error, which may have several other significant contributions (see discussion in García Pérez et al. 2009).

As expected, the 3D analysis yields systematically lower ^{6}Li/^{7}Li isotopic ratios by up to 1.8%. For comparison, we list in the last column the 1D LTE results of A06, A08, and the 3D non-LTE results of L12 from their case (a) for the stars in common with our sample. In some cases, the agreement is very good (G271–162, HD140283), even though the analysis is based on different observational data. In other cases, we obtain significantly lower ^{6}Li/^{7}Li ratios (HD 160617, G64–12). The most striking discrepancy, this time in the opposite direction, is seen for HD 84937.

G020–024 is a special case. We have retrieved the spectra obtained by A06 from the ESO archive and re-reduced them with the current UVES pipeline. We note that all six subexposures show an unexplained 'perturbation'

in the lower red wing of the Li 670.8 nm line that cannot be fitted properly, neither with 1D LTE nor with 3D non-LTE model spectra. The best 3D non-LTE fit suggests a very high ^{6}Li content near 10% (see Fig. 4), even exceeding the 1D LTE result by A06 of 7%. In view of the poor quality of the fit, we consider this result as doubtful. It is worth mentioning that G020–024 is listed as a suspected binary in Fouts (1987); moreover, A06 report that this star shows an unusually large discrepancy between the photometric and the H_α-based $T_{\rm eff}$. Possibly, G020–024 is a spectroscopic binary whose components are of similar spectral type.

Disregarding G020–024, we are left with one formal $2\,\sigma$ detection (HD 84937), one $1\,\sigma$ detection (G275–4), and five non-detections (HD 74000, G271–162, HD 140283, HD160617, G64–12) out of the eight stars, when considering the 3D non-LTE results only. In 1D LTE, G271–162 would turn into a formal $1\,\sigma$ detection (see Tab. 5).

6. Conclusions

The ^{6}Li/^{7}Li isotopic ratio derived by fitting the Li I doublet with 3D non-LTE synthetic line profiles is shown to be 1% to 2% lower than what is obtained with 1D LTE profiles. This result implies that only 2 out of the 24 stars of the Asplund et al. (2006) sample would formally remain significant ($3\,\sigma$) ^{6}Li detections when subjected to a 3D non-LTE analysis.

In another theoretical case study we have demonstrated that the difference between 3D non-LTE and 1D LTE results increases even more if we would rely on additional 'calibration lines' to fix the residual line broadening, as advocated e.g. by A06, A08, L12. The number of possible ^{6}Li detections is thus further reduced. We conclude that the usage of additional 'calibration lines', even if carefully selected, introduces additional uncertainties rather than reducing the error of the analysis, unless the 3D non-LTE line formation is fully understood for all involved lines.

Finally, we have analyzed available high quality spectra of eight turn-off halo stars, both with 1D LTE and 3D non-LTE modeling. In most cases, the evidence for the presence of ^{6}Li is not significant. Only in the case of HD 84937 it is difficult to deny the signature of ^{6}Li. Surprisingly, L12 no longer find any significant evidence for the presence of ^{6}Li in this object, which since almost two decades has been considered as an undisputed ^{6}Li detection. From the results reported by L12, it is unclear whether the reason for this disturbing discrepancy is related to the new superior observational data or to the improved method of analysis.

We conclude that 3D model atmospheres can indeed help to solve the *second lithium problem*. In view of the 3D non-LTE results reported in this work (and by L12), it seems that the presence of ^{6}Li in the atmospheres of galactic halo stars is rather the exception than the rule, and hence does not necessarily constitute a *cosmological* problem.

Acknowledgements. We thank L. Monaco and G. Lo Curto for re-reducing the HARPS spectrum of HD 160617, P.E. Nissen for providing us with a carefully reduced UVES spectrum of G275-4, and W. Aoki for allowing us to use his HDS spectrum of HD 140283.

References

Aoki, W., Inoue, S., Kawanomoto, S., et al.2004, A&A, 428, 579

Asplund, M., Lambert, D.L., Nissen, P.E., Primas, F., Smith, V.V. 2006, (A06) ApJ, 644, 229

Asplund, M., Meléndez, J. 2008, (A08) First Stars III, AIP Conference Proceedings, 990, 342

Barklem, P.S., Belyaev, A.K., Asplund, M. 2003, A&A, 409, L1

Castelli, F. & Kurucz, R. L. 2003, in IAU Symposium 210, ed. N. Piskunov, W. W. Weiss, & D. F. Gray, 20P, arXiv:astro-ph/0405087v1

Cayrel, R., Spite, M., Spite, F., Vangioni-Flam, E., Cassé, M., Audouze, J. 1999, A&A, 343, 923

Cayrel, R., Steffen, M., Chand, H., et al. 2007, A&A, 473, L37

Cayrel, R., Steffen, M., Bonifacio, P., Ludwig, H.-G., Caffau, E. 2008, Nuclei in the

Cosmos (NIC X), PoS, availale online at http://adsabs.harvard.edu/abs/2008nuco.confE...2C

Christlieb, N. 2008, Journal of Physics G: Nuclear Physics, 35, 014001

Fouts, G. 1987, PASP, 99, 986

Freytag, B., Steffen, M., & Dorch, B. 2002, AN, 323, 213

Freytag, B., Steffen, M., Ludwig, H.-G., et al. 2012, Journal of Computational Physics, 231, 919

García Pérez, A.E., Aoki, W., Inoue, S., et al. 2009, A&A, 504, 213

Lind, K., Asplund, M., Collet, R., Meléndez, J. 2012 (L12), MSAIS, 22, 142

Ludwig, H.-G., Caffau, E., Steffen, M., Freytag, B., Bonifacio, P., & Kučinskas, A. 2009, MmSAI, 80, 708

Nissen, P.E., Asplund, M., Hill, V., D'Odorico, S. 2000, A&A357, L49

Prantzos, N. 2010, IAU Symposium, 268, 473

Prantzos, N. 2012, arXiv:1203.5662 (A&A, in press)

Sbordone, L., Bonifacio, P., Caffau, E., et al. 2010, A&A, 522, A26

Steffen, M., Cayrel, R., Boinfacio, P., Ludwig, H.-G., Caffau, E. 2010a, IAU Symposium, 265, 23

Steffen, M., Cayrel, R., Boinfacio, P., Ludwig, H.-G., Caffau, E. 2010b, IAU Symposium, 268, 215